JOURNAL OF PETROLOGY

OXFORD

The Origin of Plagiogranites: Coupled SIMS O Isotope Ratios, U–Pb Dating and Trace Element Composition of Zircon from the Troodos Ophiolite, Cyprus

Navot Morag[1]*, Tzahi Golan[2], Yaron Katzir[2], Matthew A. Coble[3], Kouki Kitajima[4] and John W. Valley[4]

[1]Geological Survey of Israel, 32 Yesha'ayahu Leibowitz St, Jerusalem 9692100, Israel; [2]Department of Geological and Environmental Sciences, Ben-Gurion University of the Negev, Be'er-Sheva 84105, Israel; [3]Department of Geological Sciences, Stanford University, 450 Serra Mall, Stanford, CA 94305, USA; [4]WiscSIMS, Department of Geoscience, University of Wisconsin, 1215 W Dayton St, Madison, WI 53706, USA

*Corresponding author. Telephone: +972-2-5314329. Fax: +972-2-5314330. E-mail: navotm@gsi.gov.il

ABSTRACT

U–Pb ages, trace element content and oxygen isotope ratios of single zircons from five plagiogranite intrusions of the Troodos ophiolite were measured to determine their crystallization age and assess the importance of fractional crystallization versus crustal anatexis in their petrogenesis. The results indicate that oceanic magmatism in Troodos took place at $94\cdot3 \pm 0\cdot5$ Ma, about 3 Myr earlier than previously recognized. Later hydrothermal alteration has affected most of the Troodos plagiogranitic rocks, resulting in growth of new zircon and/or partial alteration of zircon domains, causing slightly younger apparent crystallization ages. The new age inferred for seafloor spreading and ocean crust accretion in Troodos nearly overlaps that of the Semail ophiolite in Oman (95–96 Ma), strengthening previous indications for simultaneous evolution of both ophiolites in similar tectonic settings. Average $\delta^{18}O(Zrn)$ values in the Troodos plagiogranites range between $4\cdot2$ and $4\cdot8\textperthousand$. The lower values in this range are lower than those expected in equilibrium with mantle-derived melt ($5\cdot3 \pm 0\cdot6\textperthousand$), indicating variable contribution from hydrothermally altered, deep-seated oceanic crust in most of the Troodos plagiogranite intrusions. The inferred substantial involvement of crustal component is consistent with the existence of a shallow axial magma chamber, typical of fast-spreading mid-ocean ridge settings, within the Troodos slow-spreading ridge environment. This apparent contradiction may be reconciled by episodically intense magmatism within an otherwise slow, magmatically deprived spreading axis.

Key words: Troodos ophiolite; plagiogranites; zircon; U–Pb geochronology; oxygen isotopes; SIMS

INTRODUCTION

The oceanic crust is composed of predominantly mafic rocks, owing to its derivation from mantle peridotites whose partial melting produces basaltic melts (e.g. Klein & Langmuir, 1987). Nevertheless, felsic intrusions including diorites, trondhjemites, and tonalites, collectively known as 'oceanic plagiogranites', are common minor constituents of oceanic crust sequences recovered in drill cores and exposed in ophiolites (Coleman & Peterman, 1975; Malpas, 1979; Aldiss, 1981; Lippard et al., 1986). These felsic intrusions are characterized by relatively low K_2O content and consist mainly of albitic plagioclase and quartz with minor hornblende. Secondary minerals, including epidote, chlorite, and actinolite, are usually considered the result

of post-crystallization hydrothermal alteration (Coleman & Donato, 1979). Typical accessory minerals include Fe–Ti oxides, apatite, and often zircon (Koepke *et al.*, 2007; Cavosie *et al.*, 2009; Grimes *et al.*, 2011, 2013), which makes plagiogranites preferred targets for the application of U–Pb zircon geochronology, yielding invaluable information about the formation age of the oceanic crust in modern oceans and in ophiolites (e.g. Tilton *et al.*, 1981; Mukasa & Ludden, 1987; Schwartz *et al.*, 2005; Warren *et al.*, 2005; Grimes *et al.*, 2008). Two main processes have been suggested for the formation of plagiogranites: (1) extended differentiation of mid-ocean ridge (MOR) basaltic magma (e.g. Coleman & Donato, 1979; Malpas, 1979; Lippard *et al.*, 1986; Beccaluva *et al.*, 1999); (2) hydrous partial melting of hydrothermally altered gabbro or diabase within the zone of overlapping hydrothermal and magmatic systems (Flagler & Spray, 1991; Gillis & Coogan, 2002; Koepke *et al.*, 2007; France *et al.*, 2010; Wanless *et al.*, 2010; Brophy & Pu, 2012). It is most probable that both processes may occur in MOR settings and that both are responsible for the formation of plagiogranites in various modern oceanic environments and ophiolites worldwide (Malpas, 1979; Pedersen & Malpas, 1984; Brophy, 2009).

The Troodos ophiolite of Cyprus (Fig. 1) comprises an almost intact ∼3 km thick section of Late Cretaceous oceanic crust (Moores & Vine, 1971; Varga & Moores, 1985; Malpas *et al.*, 1989; MacLeod *et al.*, 1990; Abelson *et al.*, 2001). It includes abundant plagiogranite exposures, allowing a study of their original intrusive relations within well-preserved geometry and structures of a fossil oceanic crustal section. Some of the most compelling field and petrological evidence for the production of plagiogranite magma by partial melting of hydrous oceanic crust comes from the Troodos ophiolite, where a well-preserved contact aureole at the base of the sheeted dyke complex includes migmatites with leucocratic veins that can locally be traced to a discrete plagiogranite body (Gillis & Coogan, 2002). However, a comprehensive geochemical study by Freund *et al.* (2014) revealed considerable similarities of incompatible element ratios between plagiogranites, lavas and mafic plutonic rocks and continuous chemical trends between plagiogranites and contemporaneous mafic rocks. They concluded that fractional crystallization of mafic magma was the dominant formation process of Troodos plagiogranitic intrusions. This interpretation challenges the previous interpretation of Gillis & Coogan (2002) that leucosomes and plagiogranitic intrusions are genetically related. Freund *et al.* (2014) also identified three geochemically distinct groups of plagiogranite in Troodos: a tholeiitic-related (main) group, a boninitic-related (Spilia) group and a third (Zoopigi) group unrelated to any known mafic suite.

Here we present a detailed secondary ion mass spectrometry (SIMS) study of oxygen isotope ratios, U–Pb ages and rare earth element (REE) content of single zircons from five plagiogranite intrusions in the Troodos
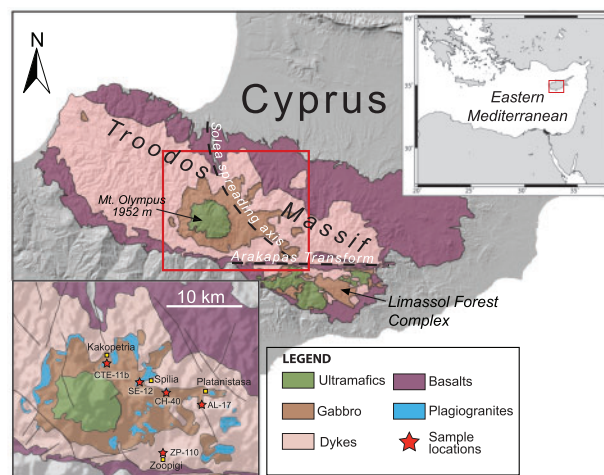
Fig. 1. Simplified geological map of the Troodos Massif of Cyprus. The inset at the lower left corner shows the geology of the Mount Olympus area and the distribution of plagiogranite intrusions and sample locations in more detail [modified after the 1:250,000 scale geological map of Cyprus (Constantinou, 1995)].

ophiolite, which represent all three plagiogranite groups defined by Freund *et al.* (2014). Zircon is a highly resistant mineral and, if undamaged by radiation, has been shown to effectively retain its original $\delta^{18}O$ value, U–Pb age and REE pattern even when subjected to later extensive hydrothermal alteration, which is almost inevitable in oceanic spreading centers (e.g. Cherniak & Watson, 2001, 2003; Valley, 2003; Valley *et al.*, 2005; Bowman *et al.*, 2011). *In situ* analysis by SIMS can reveal protracted crystallization stages preserved by individual zones within zircon crystals and thus provide a powerful tool for the study of plagiogranites origin in Troodos ophiolite and elsewhere.

GEOLOGICAL SETTING

The Troodos ophiolite of Cyprus formed along an oceanic spreading axis within the southern Neo-Tethyan realm during Turonian time, $91{\cdot}6 \pm 1{\cdot}4$ Ma, as indicated by bulk zircon U–Pb dating of Troodos plagiogranite samples (Mukasa & Ludden, 1987). It is considered one of the best preserved on-land sections of oceanic crust and includes a complete and intact sequence of pelagic sediments, pillow lavas, sheeted dykes, felsic to ultramafic plutonic rocks and mantle rocks, which is comparable with that deduced for modern MOR setting from geophysical data (e.g. Gass, 1968). However, geochemical and textural evidence, including the occurrence of boninites (distinctive high-Mg andesites), characteristic mineral crystallization sequence, variable enrichment in large ion lithophile elements (LILE) and depletion in high field strength elements (HFSE), indicates that the Troodos ophiolite, like many other major ophiolites around the world, formed in a suprasubduction-zone (SSZ) setting rather than in a 'typical' MOR setting (e.g. Cameron *et al.*,

1979; Pearce *et al.*, 1984; Pearce & Robinson, 2010; Dilek & Furnes, 2014).

The current structure of the Troodos massif (Fig. 1) is a WNW–ESE-trending antiform that formed during late Miocene to early Pleistocene convergence of the African and Anatolian plates along the Cyprean trench (Robertson, 1977; McCallum & Robertson, 1990; Kinnaird *et al.*, 2011; Morag *et al.*, 2016). Pillow lavas are exposed along the antiform flanks and sheeted dykes are exposed along most of its axis. The deeper plutonic and mantle sequences are exposed at the highest elevations around Mt Olympus (1952 m above sea level), between the Solea Graben, thought to represent a former spreading axis (Varga & Moores, 1985), to the north, and the fossil oceanic Arakapas transform fault to the south (Abelson *et al.*, 2001). The same rock units are also exposed in the Limassol Forest area, south of the Arakapas transform fault, where, in contrast to the major Troodos massif, the oceanic crust section was intensely deformed (MacLeod *et al.*, 1990) (Fig. 1).

The Troodos mantle sequence consists of partially serpentinized harzburgite, dunite and pyroxenite. These rocks are overlain by a plutonic sequence composed principally of layered and isotropic gabbro, including some cumulate ultramafic layers and veins and pods of plagiogranites. The plagiogranites are most common in the upper part of the plutonic sequence below its contact with the sheeted dyke complex, where they may form small (up to a few km^2 sized) exposures. Smaller (<500 m^2) plagiogranite bodies are intruded into the base of the sheeted dykes and also occur as felsic dykes concordant with the mafic sheeted dyke complex. In places, a metamorphic aureole, composed of pyroxene and hornblende hornfels and containing migmatite textures, is developed at the base of the sheeted dyke complex, along its contact with the gabbroic plutons. Some of the leucocratic veins within the migmatites can be traced to a discrete plagiogranite body, although in most cases this relationship is not easily observed (Gillis & Coogan, 2002). The plagiogranites are locally altered to epidote–quartz and chlorite assemblages, generated by syn- to post-magmatic auto-metasomatism and by later hydrothermal, seawater-derived fluid flow, which supports their formation within an active spreading environment (Kelley *et al.*, 1992; Gillis, 2002; Anenburg *et al.*, 2015).

The sheeted dyke complex and the overlying pillow lavas section consists mainly of tholeiitic rocks, but rare boninites also occur in some areas, usually above the tholeiitic lavas (Cameron *et al.*, 1979; Robinson *et al.*, 1983; Cameron, 1985; Staudigel *et al.*, 2000; Pearce & Robinson, 2010; Osozawa *et al.*, 2012). Boninites are considered typical of emergent fore-arc settings and their existence together with moderate-Fe, rather than high-Fe, tholeiites in the Troodos ophiolite was taken as an indication of subduction initiation, slab-edge tectonic setting (Pearce & Robinson, 2010). The scattered occurrence of boninitic rocks and their typically higher stratigraphic position were interpreted to represent a late,

off-axis magmatic stage (Freund *et al.*, 2014). Most of the Troodos plagiogranitic intrusions studied by Freund *et al.* (2014) have geochemical similarities to the major tholeiitic magmas, which formed most of the lavas and sheeted dyke complex of the Troodos crust. One large plagiogranitic pluton near the village of Spilia was related to the late-stage, off-axis boninitic lavas, based on its distinct incompatible trace element pattern, which is more comparable with those of the boninitic lavas. Plagiogranitic dykes and small intrusions, which alternate with aphyric mafic dykes near the village of Zoopigi, are incompatible element enriched compared with the other tholeiite- and boninite-related plagiogranites and were not related with any of the Troodos mafic suite (Freund *et al.*, 2014). The Zoopigi plagiogranites have higher Zr content (64–141 ppm) compared with the boninitic (≤63 ppm) and tholeiitic (40–95 ppm) types (Freund *et al.*, 2014), and are therefore termed here 'Zr-rich plagiogranites'.

SAMPLING

Twenty samples of plagiogranite were collected from outcrops around Mount Olympus, with only five of the eastern samples yielding zircon. The scarcity of zircon in the Troodos plagiogranites was previously noted by Mukasa & Ludden (1987), who succeeded in obtaining sufficient zircon for bulk thermal ionization mass spectrometry (TIMS) analysis from only two rocks of their total sampled suite. Similarly, zircon was not identified in thin section ($n = 60$) nor by X-ray diffraction (XRD) analysis ($n = 10$) of the Troodos plagiogranites studied by Freund *et al.* (2014). Most of the zircon-bearing intrusions studied here occur along the gabbro–sheeted dyke transition zone of the Troodos Ophiolite; one sample (ZP-110) is located within the sheeted dykes section (Fig. 1). The SiO$_2$ content of the studied samples was determined using XRF and ranges between 60 and 75 wt%. The locations of the studied samples and their SiO$_2$ contents are given in Table 1. The following is a brief description of the outcrops and field relations of the studied intrusions.

Sample AL-17 was collected along the Alona–Polystipos road from a small outcrop (several 10 m^2 sized) composed of a grey plagiogranite body intrusive into diabase. Diabase xenoliths are abundant within the plagiogranitic or dioritic rock (Fig. 2a). Sample CH-40 was taken from a small felsic intrusion (~50 m^2 exposure) at the northeastern outskirts of the village of Chandria. Along a road cut (Fig. 2b) an olivine-gabbro country rock is repeatedly intruded by younger intrusions. The earliest of these is a light plagiogranite body (sample CH-40), composed of quartz, plagioclase and epidote. Both gabbro and plagiogranite are intruded by a number of subvertical microgabbroic dykes that show well-developed chilled margins, followed by a series of vertical diabase dykes. Sample CTE-11B was collected along the Kakopetria–Agios Nikolaos road, from a small outcrop (~200 m^2) where grey–pinkish plagiogranite of

Table 1: Summary of data for the studied samples

Sample	Intrusion	Geographical coordinate	Group*	SiO$_2$ (wt%)	U–Pb age (Ma)			δ^{18}O (‰ VSMOW)				
					Wtd. mean (95 % conf.)	MSWD	n†	Av.	2SD	Min.	Max	n (grains)
Al-17	Alona–Platanistassa	N34·9268/E33·0483	Tholeiitic	65·1	91·0 ± 2·1	8·1	9	4·8	0·3	4·5	5·2	12 (10)
CH-40	Chandria	N34·9414/E32·9960	Tholeiitic	71·0	92·5 ± 1·4	2·9	9	4·5	0·3	4·3	4·7	8 (6)
CTE-11B	Kakopetria	N34·9810/E32·8950	Tholeiitic	59·5	91·1 ± 3·7	2·6	4	4·2	0·2	4·1	4·3	4 (3)
SE-12	Spilia	N34·9633/E32·9609	Boninitic	75·1	90·2 ± 6·8	0·1	2	4·7	0·3	4·5	4·8	11 (11)
ZP-110	Zoopigi	N34·8703/E32·9928	IE-enriched	74·3	94·3 ± 0·5	1·2	25	4·5	0·2	4·4	4·7	17 (15)

*Troodos plagiogranite groups according to the classification of Freund *et al.* (2014).
†Each analysis represents a different grain.

Fig. 2. Field relations at the studied plagiogranite sample localities. (a) AL-17 (Alona–Polystipos road), angular diabase xenoliths hosted in plagiogranite; (b) CH-40 (near Chandria), plagiogranite intruded into olivine gabbro and in turn injected by microgabbro dykes and late diabase dykes; (c) CTE-11B (Kakopetria–Agios Nikolaos road), plagiogranite body injected by aphyric mafic dykes, later rotated; (d) Spilia intrusion (SP-12), stoped gabbro xenoliths at the contact of a large plagiogranite intrusion; (e) ZP-110 (near Zoopigi), small plagiogranite body intrusive into the aphyric mafic dykes.

variable grain size is intruded by mafic aphyric dykes, later rotated to subhorizontal position (Fig. 2c). Parts of the plagiogranite body seem highly altered, containing a significant amount of epidote. Sample SP-12 was collected from the Spilia plagiogranite—a relatively large intrusion (a few km^2) located at the gabbro–sheeted dykes transition zone close to the village of Spilia. The Spilia intrusion contains numerous mafic xenoliths, up to 1 m in diameter, along its margins (Fig. 2d), interpreted as stoped blocks of gabbro incorporated into the plagiogranite during its emplacement. The Spilia intrusion is rarely intruded by dykes and was therefore considered as late compared with the other plagiogranites (Freund *et al.*, 2014). Sample ZP-110 was sampled east of the village of Zoopigi from a small light grey granite body intruded into mafic dykes; adjacent similar plagiogranites are intruded by late aphyric dykes (Fig. 2e). The Zoopigi plagiogranites are intensely tectonized by faults and shear zones, possibly because of their proximity to the Arakapas Fault zone (Freund *et al.*, 2014).

ANALYTICAL METHODS

Sample preparation

Zircon grains were separated from the plagiogranite samples by mechanical crushing followed by standard separation techniques including wet sieving (60–300 μm), heavy liquid (tetrabromoethane; ∼2·95 g cm^{-3}) and Frantz magnetic separator. Individual zircon grains were hand-picked under a stereomicroscope and mounted in epoxy along with a set of U–Pb (R33/TEMORA-2) and oxygen isotope (KIM-5) zircon standards. The grains were polished to mid-section to expose the grains' interiors. All grains were imaged prior to analysis using scanning electron microscopy (SEM) with cathodoluminescence (CL) and backscattered electron (BSE) detectors to evaluate zoning patterns and identify mineral inclusions and cracks (Fig. 3, Supplementary Data Fig. S1; supplementary data are available for downloading at http://www.petrology.oxfordjournals.org).

SIMS U–Pb isotope and trace element analysis

Zircon U–Th–Pb isotope and trace element analyses were performed by SIMS at Stanford University using a sensitive high-resolution ion microprobe with reverse geometry (SHRIMP-RG). Secondary ions were sputtered from the target spot using an O_2^- primary ion beam, which was accelerated at 10 kV and had an intensity varying from 3·0 to 4·0 nA. The primary ion beam spot had a diameter between 22 and 28 μm and a depth of ∼1–3 μm for the analyses performed in this study. Trace elements (Y, Hf, REE) were measured briefly (typically 0·2–3 s per mass) before the geochronology peaks, and in mass order. All peaks were measured on a single ETP$^®$ discrete-dynode electron multiplier operated in pulse counting mode. Zircon trace elements and

^{206}Pb/^{238}U ages were calculated following the methods of Watts *et al.* (2016). Calculated ages for zircon were standardized relative to zircon standards R33 or TEMORA-2 (^{206}Pb/^{238}U ages = 416·8 and 419·3 Ma, respectively; Black *et al.*, 2004), which were analyzed repeatedly throughout the duration of the analytical session. Measured U, Th and trace element content were calibrated using well-characterized, homogeneous zircon standard MAD-green (4196 ppm U; Coble *et al.*, 2018), which was mounted on a separate setup mount. Measured REE content was normalized to chondrite values given by McDonough & Sun (1995).

EPMA chemical analysis

Zircon chemical analyses were performed by electron probe micro-analysis (EPMA) using a JEOL JXA-8230 Superprobe system at the Hebrew University of Jerusalem. The amounts of Zr, Si, P, Hf, Y, Ce and Yb were measured by wavelength-dispersive X-ray spectrometry (WDS) using an accelerating voltage of 15 kV, probe current of 15 nA and a fully focused beam. Each analysis spot was measured for 60 s per element, with background counting times set to half of the respective peak counting times. Standards used include natural minerals (olivine, apatite, rutile and monazite) as well as synthetic materials (yttrium-garnet). Zircon formulae were calculated on the basis of four oxygens per formula unit.

Oxygen isotope analysis

Zircon oxygen isotope ratios were measured at the University of Wisconsin–Madison SIMS laboratory (WiscSIMS) using a CAMECA IMS-1280 during a single analytical session. Samples were re-polished prior to the analysis to remove the U–Pb analysis spots. Additional CL imaging was performed to re-check the CL patterns after polishing. Measurements were made with a focused Cs$^+$ ion beam with an intensity of 1·8–2·1 nA and a spot size of ∼10 μm diameter and 1 μm depth, following the methods described by Kita *et al.* (2009). Four analyses of the KIM-5 zircon standard were performed routinely at the beginning of each session, and repeatedly after every 10 unknowns. The bracketing sets of eight analyses of KIM-5 (δ^{18}O = 5·09 ‰ VSMOW; Valley *et al.*, 2003) were used to correct for instrumental mass fractionation. The spot-to-spot reproducibility (external precision) for individual brackets of KIM-5 ranged between 0·17 and 0·28 ‰ (2SD) during the analytical session. Following analysis, all SIMS pits were re-examined by SEM in BSE mode and assigned a pit quality value based on their shape and the presence of any cracks or mineral inclusions, ranging from one (good; clear regular shape) to five (poor; intersects cracks, inclusions or of irregular shape).
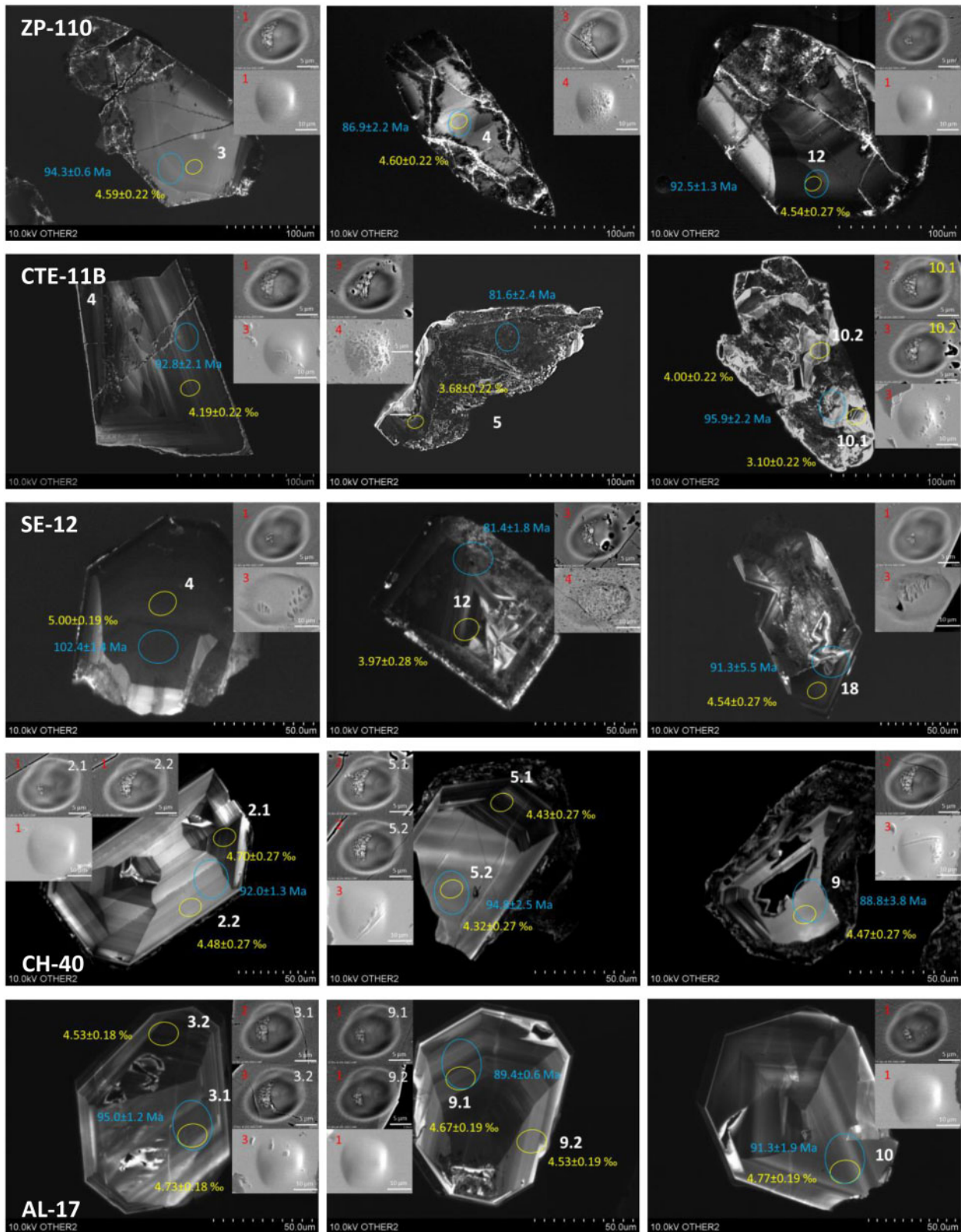
Fig. 3. Cathodoluminescence (CL) and backscattered electron (BSE) images of selected zircon grains and analysis pits. Analysis spot numbers are given in white. Yellow and cyan open circles indicate the location of oxygen and U–Pb isotopic analyses, respectively. The analytical results are given in the adjacent numbers with matching colors. The numbers in red over the analysis pits images indicate the assigned pit quality value, ranging from one (good; clear regular shape) to five (poor; intersects cracks, inclusions or of irregular shape).

RESULTS

U–Pb geochronology and trace element composition of zircon

A total of 73 SHRIMP analyses were performed on zircon grains separated from the five plagiogranite samples. Studied zircons were mostly euhedral to subhedral, typically 100–150 μm long grains, showing simple oscillatory and sector zoning typical of magmatic zircon. Many of the grains have 'porous' domains with irregular CL patterns, found mostly along cracks and grain boundaries as overgrowths (Fig. 3, Supplementary Data Fig. S1). These domains were generally avoided as they are interpreted to form by secondary hydrothermal alteration or precipitation (e.g. Grimes *et al.*, 2009; Schwartz *et al.*, 2010). However, porous textures were often recognized in post-analysis inspection of the analysis pits (Fig. 3; Supplementary Data Fig. S1). A complete set of the U–Pb geochronological data and trace element geochemical data from the SHRIMP analysis is given in Supplementary Data Table S1.

Most of the analyzed zircons yielded relatively high Y and REE content, ranging from a few weight per cent Y and total REE, up to ~16 wt% Y and ~8 wt% total REE in some zircons from sample SE-12 of the Spilia intrusion (Supplementary Data Table S1). Previous studies have shown that zircons from oceanic crust are typically Y- and heavy REE (HREE)-enriched, with values ranging up to ~8 and ~2 wt%, respectively (Grimes *et al.*, 2007). However, extreme values such as those measured in the Spilia zircons were previously not reported (Fig. 4). To verify these results, we have re-measured the trace and major element composition of zircon using EPMA. Although the EPMA system is less sensitive and has a higher detection limit for trace elements compared with the SHRIMP, it is less susceptible to matrix-induced instrumental bias arising from chemical and/or structural differences between the analyzed sample and the calibration standard. The complete set of major and trace element geochemical data obtained by EPMA is given in Supplementary Data Table S2. For most samples the SHRIMP and EPMA results are consistent, with Y content varying by no more than 2 wt% (20 000 ppm). Conversely, the extreme Y and Yb SHRIMP values in sample SE-12 are not reproduced by EPMA, which yielded maximum Y and Yb values of ~6 and ~1·6 wt%, respectively (Supplementary Data Table S2). This suggests that some SE-12 zircons may have different structure and/or chemical composition from that of the SHRIMP calibration zircon standard, which prevents their accurate analysis. CL imaging of the zircons with irreproducible SHRIMP and EPMA data revealed no unusual textures and they usually display fine oscillatory zoning typical of magmatic zircon (Fig. 3; Supplementary Data Fig. S1). Likewise, EPMA confirms that sample SE-12 zircons have characteristic zircon stoichiometry with only up to ~4 mol% xenotime endmember [(Y,HREE)PO₄; calculated from the amount of P

in the tetrahedral site], similar to zircons from the other studied samples. However, high SHRIMP Y content in sample SE-12 zircons is found to correlate with high $^{16}OH/^{16}O$ ratio measured for the same grains during the O isotope analysis (Supplementary Data Table S3). This correlation suggests that these zircons are radiation damaged (metamict) and have amorphous or partly amorphous structure, which differs from that of the crystalline zircon calibration standard (Wang *et al.*, 2014). Higher Y SHRIMP values in sample SE-12 are generally correlated with older U–Pb ages (Supplementary Data Table S1), indicating that these older ages are also likely to result from this sample–standard crystalline mismatch. Accordingly, all zircons for which the difference between SHRIMP-measured and EPMA-measured Y values was greater than 2 wt% are suspected as metamict zircons and their SHRIMP geochemical and geochronological data were therefore rejected.

The measured $^{206}Pb/^{238}U$ and $^{207}Pb/^{206}Pb$ ratios (not corrected for common Pb) of zircons from the studied samples are plotted on Tera–Wasserburg concordia diagrams in Figure 5. Reported sample ages are weighted mean $^{238}U/^{206}Pb$ ages corrected for common Pb using measured $^{207}Pb/^{206}Pb$ (Ireland & Williams, 2003) assuming common $^{207}Pb/^{206}Pb$ from Stacey & Kramers (1975).

Sample ZP-110, with the largest dataset of 25 analysis points, yielded ($^{207}Pb_c$-corrected) $^{206}Pb/^{238}U$ dates for individual spot analyses ranging from 86·9 ± 4·8 (2σ) to 95·9 ± 2·4 Ma (Fig. 5a). The four youngest dates, <90 Ma, correlate with porous textured pits (e.g. Fig. 3; Supplementary Data Fig. S1), suggesting later hydrothermal-alteration or growth (marked by red ellipses and error bars). After the rejection of these four young dates the sample yielded a weighted mean $^{206}Pb/^{238}U$ age of 94·3 ± 0·5 (2SD) Ma (MSWD = 1·18). Applying these same criteria to other samples with fewer data points, we have omitted from the average age calculation all analysis spots that have intersected porous zircon domains (pit quality value >3).

After the rejection of five analysis spots that intersected porous domains, sample CTE-11B yielded a weighted mean $^{206}Pb/^{238}U$ age of 91·1 ± 3·7 Ma (MSWD = 2·6) for the remaining four grains. The rejected porous grains have younger dates, between 79·6 ± 3·3 and 87·1 ± 6·5 Ma, with increased common-Pb component (Fig. 5b). The same analysis spots also show high La concentration, low (Sm/La)_N ratio and low Ce anomaly typical of hydrothermal zircon (Hoskin, 2005; Fig. 6). These newly precipitated or hydrothermally altered zircons yielded a weighted mean $^{206}Pb/^{238}U$ age of 81·0 ± 2·0 Ma (MSWD = 1·1), which may reflect the time of hydrothermal alteration event. The oldest grain in the sample, with a $^{206}Pb/^{238}U$ date of 95·9 ± 4·4 Ma, is also suspected as hydrothermal zircon based on its low (Sm/La)_N ratio (nevertheless, it did not show a distinctive porous texture and was therefore not excluded from the weighted mean age calculation).
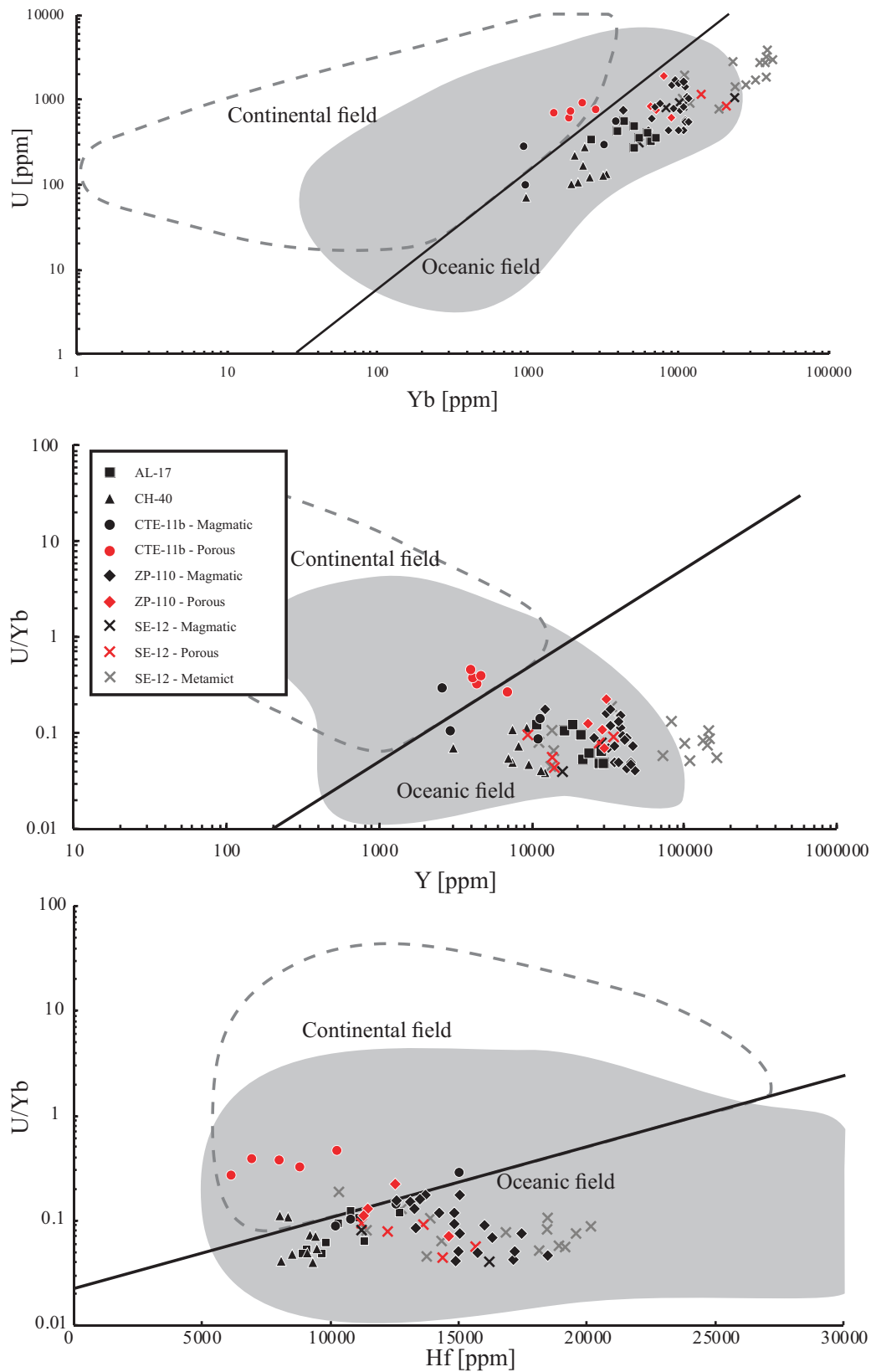
Fig. 4. Geochemical discriminant diagrams for oceanic zircon after Grimes *et al.* (2007). Plots include SIMS data for analyzed zircons from all plagiogranite intrusions in this study. Continuous line represents the lower boundary of continental field, based on >1500 analyses of Phanerozoic and Archean continental zircon (Grimes *et al.*, 2007).
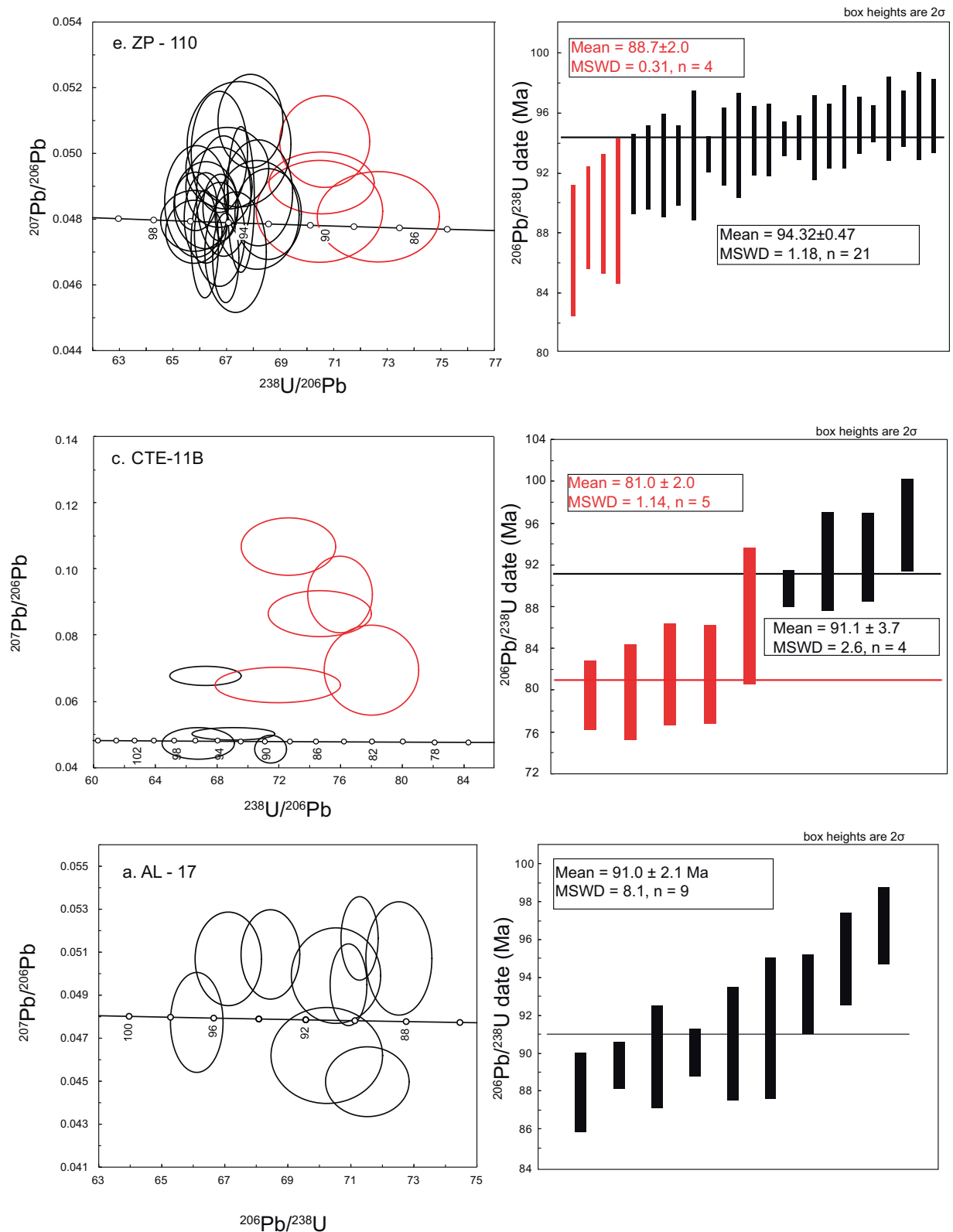
Fig. 5. Tera–Wasserburg concordia diagrams and calculated weighted mean (^{207}Pb$_c$-corrected) ^{206}Pb/^{238}U ages for studied plagiog-ranite samples. Ellipses on the concordia diagrams represent uncorrected zircon U–Pb ratios. Red ellipses and bars represent hydrothermal zircons or zircon domains recognized by their porous textures (pit quality value >3). Grey ellipses and bars represent zircons or zircon domains suspected as metamict zircon. Error ellipses and bars are 2σ. The data were plotted and calculated using the Isoplot program of Ludwig (2012).
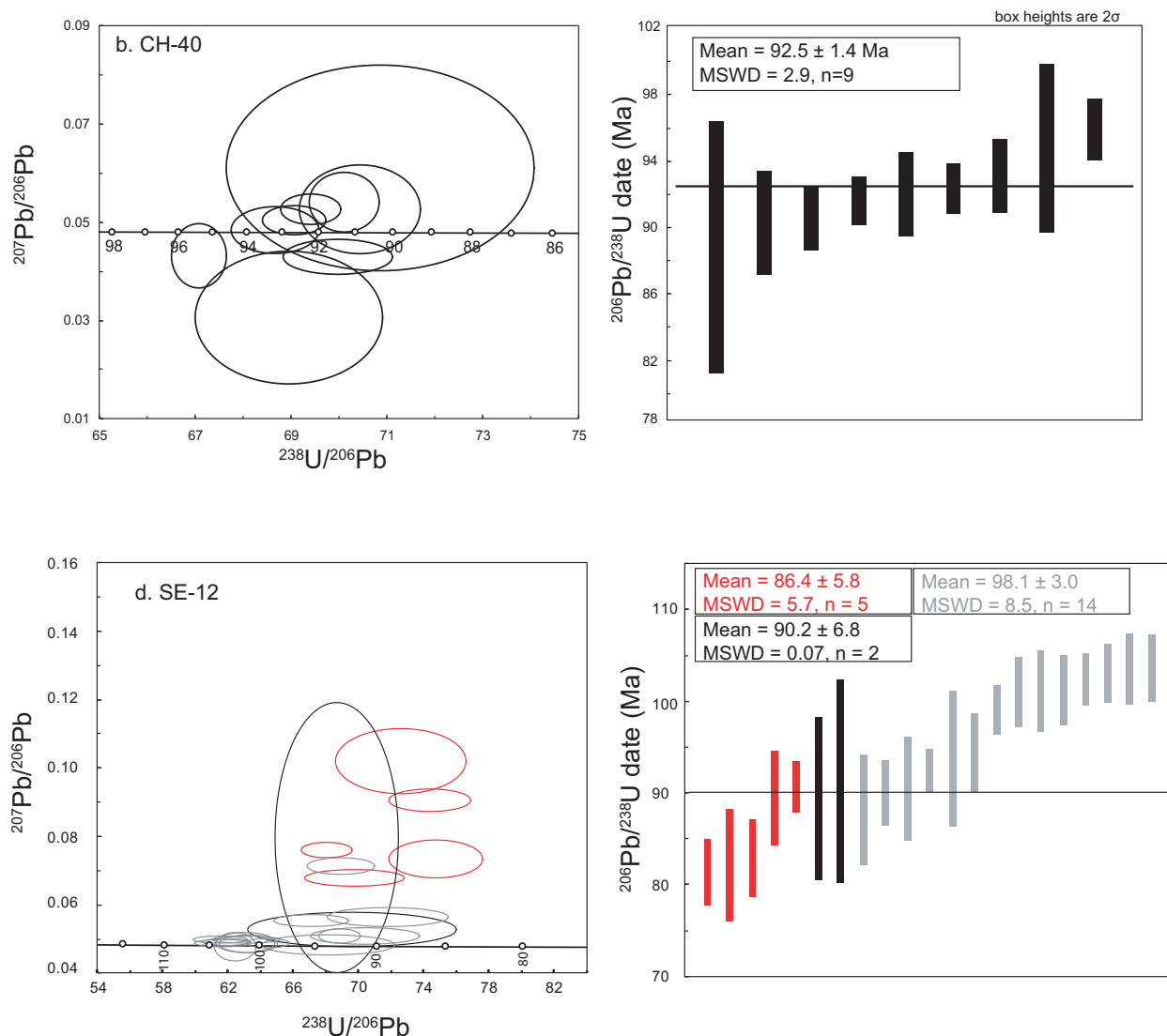
Fig. 5. Continued.

Sample AL-17 yielded $^{206}Pb/^{238}U$ dates for individual spot analyses ranging from 88.0 ± 2.1 to 96.8 ± 2.0 Ma. The weighted mean $^{206}Pb/^{238}U$ age of 91.0 ± 2.1 Ma calculated for this sample has a high mean square weighted deviation (MSWD) value of 8.1 (Fig. 5c). We interpret this scatter to represent post-crystallization Pb loss. However, no indications for hydrothermal origin, in the form of porous textures and/or low $(Sm/La)_N$ ratios, were found in the analyzed spots, so we conservatively included all analyses in the calculated weighted mean age.

Sample CH-40 yielded a weighted mean $^{206}Pb/^{238}U$ age of 92.5 ± 1.4 Ma (Fig. 5d). The individual dates in this sample show a slight scatter (MSWD = 2.9) that may indicate late Pb loss. However, we have found no indications for hydrothermal origin in this sample.

Sample SE-12 yielded a wide range of $^{206}Pb/^{238}U$ dates for individual spot analyses ranging from 81.4 ± 3.6 to 103.6 ± 3.8 Ma (Fig. 5e). The older dates in

this sample (14 total) are suspected as metamict zircon, based on their correlation with high $^{16}OH/^{16}O$ ratio and irreproducible Y and HREE content (see discussion above at the beginning of this section), and were therefore rejected from further processing. Of the remaining seven analysis spots, five intersected porous zircon domains and were excluded as suspected of hydrothermal origin. The two remaining grains, with non-porous analysis pits, yielded a weighted mean $^{206}Pb/^{238}U$ age of 92.0 ± 6.8 Ma. All analysis spots in this sample, porous and non-porous, show high La concentration and low $(Sm/La)_N$ ratio, typical of hydrothermal zircon (Hoskin, 2005; Fig. 6a).

Oxygen isotope ratios

A total of 101 analyses were performed on 77 zircon grains separated from the five plagiogranite samples. Oxygen isotope analyses were performed on the same
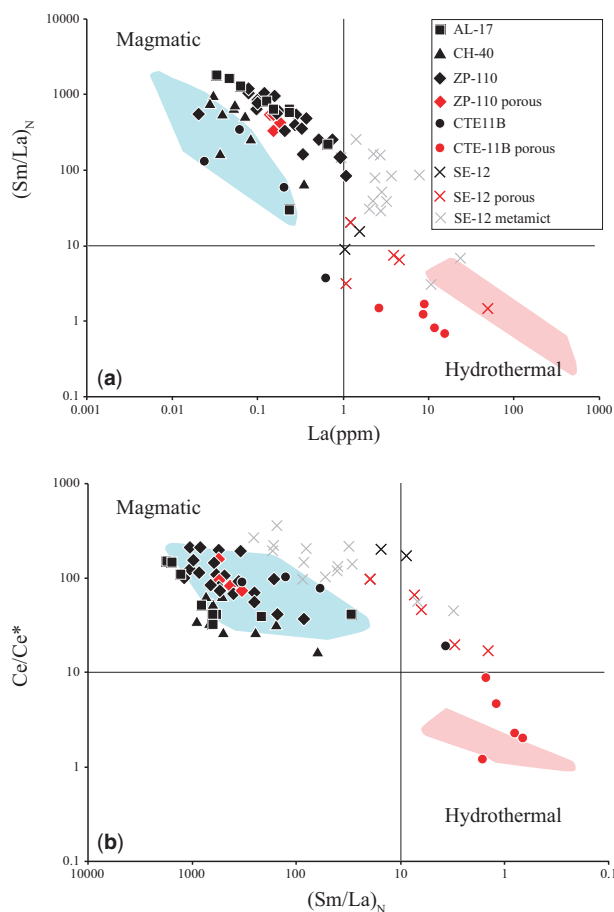
Fig. 6. (a) $(Sm/La)_N$ ratio vs La (ppm) and (b) Ce/Ce* vs (Sm/La)$_N$ ratio discrimination plots for magmatic and hydrothermal zircon after Hoskin (2005). Plots include data for dated zircons from all plagiogranite intrusions in this study. The light blue and pink shaded areas indicate the field of magmatic and hydrothermal zircon data, respectively (Hoskin, 2005).

CL-domain of the grain targeted by the U–Pb and REE analyses. In some grains multiple analyses were performed on different domains within the grain to test heterogeneity. The complete oxygen isotope dataset for the studied samples is given in Supplementary Data Table S3. Based on SEM imaging of analytical pits, nearly half (49 out of 101) of the analyses were rejected because they overlapped porous domains, inclusions or cracks (pit quality value >2). These spots may not represent the actual $\delta^{18}O$ of the zircon crystal owing to analysis of non-zircon phases. No correlation was found between individual analysis-spot $\delta^{18}O$ values and background corrected $^{16}OH/^{16}O$ ratios, in any of the studied samples (Supplementary Data Table S3).

Measured $\delta^{18}O$ values in zircons from all the studied samples are presented in Figure 7. A summary of average, minimum and maximum $\delta^{18}O$ values of clean analytical pits in all the studied samples is given in Table 1, together with the weighted mean $^{206}Pb/^{238}U$ ages. Zircons from most samples exhibit $\delta^{18}O$ ranges of 0·6 ‰ or less, nearly similar to that of the bracketing standard, which means that the grains within each sample are not
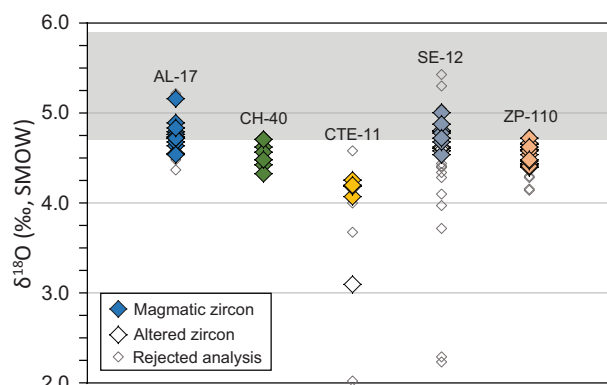
Fig. 7. Measured $\delta^{18}O$ for zircons from the studied plagiogranitic samples. Each filled diamond represents a single analysis spot. Open symbols represent hydrothermal zircons recognized by $(Sm/La)_N < 10$. Analysis spots rejected owing to identification of cracks, inclusions or irregular analysis pit shape are marked by smaller open grey diamonds. The shaded horizontal band represents $\delta^{18}O(Zrn)$ values in high-temperature equilibrium with the mantle (5·3 ± 0·6 ‰, 2SD; Valley *et al.*, 1998, 2005).

distinguishable from being perfectly homogeneous. All samples, excluding CTE-11B, yielded similar average $\delta^{18}O(Zrn)$ values between 4·5 ± 0·2 (2SD) and 4·8 ± 0·3 ‰, which plot along the lower margin of the range of $\delta^{18}O(Zrn)$ values expected in high-temperature equilibrium with uncontaminated mid-ocean ridge basalt (MORB) [5·3 ± 0·6 ‰ (2SD); Valley *et al.*, 2005]. Sample CTE-11B yielded an average $\delta^{18}O(Zrn)$ value of 4·2 ± 0·2 ‰, appreciably lower than the MORB-equilibrium $\delta^{18}O(Zrn)$ range (Fig. 7). The oldest grain in this sample, suspected as hydrothermal zircon based on its low $(Sm/La)_N$ ratio, yielded an exceptionally low value of 3·1 ± 0·2 ‰, which was not included in the average $\delta^{18}O(Zrn)$ calculation. Other hydrothermal zircon domains identified in this sample were either not targeted for $\delta^{18}O$ analysis or rejected following SEM imaging of the analytical pit because of their porous, inclusion-rich texture. Similarly, most $\delta^{18}O$ analyses on hydrothermal zircon domains from sample SE-12 were rejected because of their porous, inclusion-rich texture.

DISCUSSION

The age of ocean crust magmatism in Troodos ophiolite

Trace element classification diagrams for the provenance of Troodos zircons are shown in Figure 4 (after Grimes *et al.*, 2007). Except for the hydrothermal zircons of sample CTE-11B, zircons from all Troodos plagiogranite samples plot within the ocean crust zircon field, confirming their oceanic origin.

Weighted mean $^{206}Pb/^{238}U$ ages calculated for most samples (AL-17, CH-40, CTE-11B and SE-12) range between 90·2 ± 6·8 and 92·5 ± 1·4 Ma, all consistent with the age of 91·6 ± 1·4 Ma obtained by TIMS by Mukasa & Ludden (1987) for their Troodos plagiogranite samples. However, in all these samples we have found

indications for late hydrothermal zircon alteration or growth and Pb loss. Sample ZP-110 from the Zoopigi intrusion yielded an older age of 94.3 ± 0.5 Ma, which is the most reliable crystallization age because it is based on 21 spot analyses with no excess scatter (MSWD = 1.2, after the rejection of four porous analysis spots). We therefore suggest that the actual age of oceanic magmatism in Troodos should be dated at 94.3 ± 0.5 Ma, rather than the commonly cited zircon U–Pb age of 91–92 Ma obtained by Mukasa & Ludden (1987). It is most probable that the bulk zircon populations analyzed by Mukasa & Ludden (1987) included hydrothermally altered zircons, new growth of hydrothermal zircons, and/or zircon domains that have undergone Pb loss, which are shown here to be very common in the Troodos plagiogranites [it was not specified by Mukasa & Ludden (1987) whether they used any mechanical or chemical abrasion method to try to remove such zircon domains]. Osozawa *et al.* (2012) have reported a whole-rock Ar–Ar age of 90.6 ± 1.2 Ma for one tholeiitic pillow lava sample and an age of 55.5 ± 0.9 Ma for a boninitic pillow lava sample. We suspect that these whole-rock Ar–Ar ages are also likely to have been reset during later hydrothermal alteration, despite the good plateaux seen in their Ar release spectra (e.g. Baksi, 2006).

The older age inferred here for oceanic crust formation in the Troodos ophiolite is closer to the age of oceanic crust formation in the Semail ophiolite of Oman (95–96 Ma; Rioux *et al.*, 2016). This age similarity further strengthens the tectonic link suggested between the Troodos, Semail and other late Cretaceous peri-Arabian ophiolites along the Tethyan belt, which were previously suggested to have developed within a laterally continuous arc–trench rollback system in the Southern Tethys at about the same time (Robertson, 2002; Dilek & Flower, 2003). All these Cretaceous ophiolites display structural field evidence for original seafloor spreading tectonics and composite extrusive and intrusive sequences with different magmatic plumbing systems, collectively pointing to oceanic crust formation in an extended arc–forearc setting (Dilek & Furnes, 2009).

## Generation of the plagiogranite magmas: fractional crystallization versus crustal remelting

Zircon is selected here to study the oxygen isotope ratios of Troodos plagiogranites as it is highly retentive of magmatic $\delta^{18}O$, unlike whole-rock (WR) samples and most minerals, which have been shown to be more easily affected by high- and low-temperature alteration (this study and data from Kelley *et al.*, 1992; Freund *et al.*, 2014; Anenburg *et al.*, 2015). The average $\delta^{18}O(Zrn)$ values in the studied samples plot either along the lower margin of the range of $\delta^{18}O(Zrn)$ values expected in high-temperature equilibrium with uncontaminated MORB [$5.3 \pm 0.6\%$ (2SD); Valley *et al.*, 2005] or well below it (sample CTE-11B, Table 1; Fig. 7). These lower than mantle zircon values require the

involvement of crustal anatexis in the production of the plagiogranitic melts. This is because in typical ocean crust, interactions between mafic rocks and seawater-derived fluids at high temperature will shift $\delta^{18}O(WR)$ toward lower values, owing to the small isotopic fractionation ($\Delta^{18}O \sim 0-1\%$) between hydrous fluids and rocks at $T \geq 300 °C$. Altered rocks with lower-than-MORB $\delta^{18}O(WR)$ values are characteristically observed near the transition zone between the sheeted dyke complex and the upper gabbros, where most plagiogranitic intrusions occur (e.g. Muehlenbachs & Clayton, 1976; Gregory & Taylor, 1981; Eiler, 2001). Melts produced by anatexis of hydrothermally altered crust may be subsequently assimilated by mafic magmas (which usually provide the heat needed for anatexis) or may coalesce to form discrete felsic plutons. Nevertheless, assessing the actual amount of altered crust component in the plagiogranitic melts from their $\delta^{18}O(Zrn)$ values is not straightforward and strongly relies on the selected zircon–melt (or WR) isotope fractionation factor [$\Delta^{18}O(Zrn–WR)$] and the assumed $\delta^{18}O$ values of both the altered crustal component and the mantle-derived MORB component.

To use zircon as a proxy to estimate the $\delta^{18}O$ of the bulk magma $\Delta^{18}O(Zrn–WR)$ must be known at various magmatic temperatures and whole-rock compositions. Using mineral modes, oxygen isotope fractionations, wt% SiO_2, $\delta^{18}O(Zrn)$ and estimated solidus temperatures of ~ 300 plutonic rocks from the Sierra Nevada Batholith, Lackey *et al.* (2008) formulated the equation

$$\Delta^{18}O(Zrn–WR) = \delta^{18}O(Zrn) - \delta^{18}O(WR) \\ \approx -0.0612[SiO_2] + 2.5. \quad (1)$$

Using this relationship, which was derived for wet magmas, and the average measured $\delta^{18}O(Zrn)$ values and SiO_2 content, the original $\delta^{18}O(WR)$ values of the Troodos plagiogranitic magmas are calculated to range from 5.3 to 7.1‰ (Fig. 8; Supplementary Data Item S1). Somewhat different $\Delta^{18}O(Zrn–WR)$ versus wt% SiO_2 relations were modelled by Bucholz *et al.* (2017) for dry magmas based on incremental calculation of mineral modes, oxygen isotope fractionations, WR chemistry, and estimated liquidus temperatures in evolving tholeiitic melt, as observed in the Upper and Upper Main Zone (UUMZ) tholeiite series of the Bushveld Igneous Complex (Vantongeren *et al.*, 2010). Using these modelled $\Delta^{18}O(Zrn–WR)$ values in accordance with average measured $\delta^{18}O(Zrn)$ values and SiO_2 content, the original $\delta^{18}O(WR)$ values of the Troodos plagiogranitic magmas are calculated to range from 4.8 to 6.8‰ (Fig. 8). For a given SiO_2 content, these fractionations are 0.5–1‰ lower than those predicted by the formulation of Lackey *et al.* (2008). The major difference between the two $\Delta^{18}O(Zrn–WR)$ calculation models stems from the hydrous composition of the calc-alkaline magmas of the Sierra Nevada Batholith studied by Lackey *et al.* (2008) and the use of solidus temperature estimates versus the dry composition of the Bushveld UUMZ
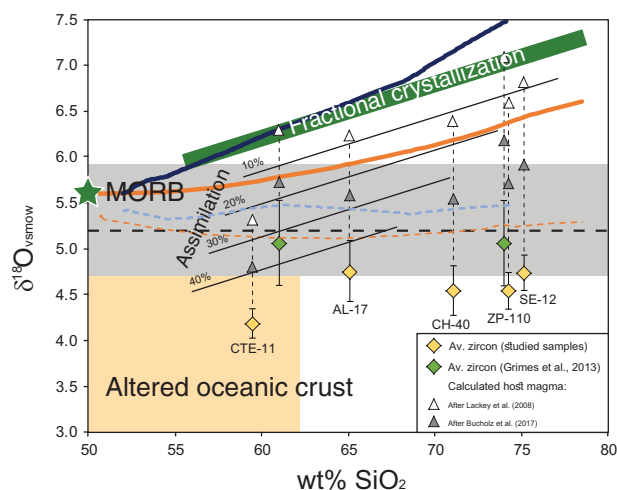
Fig. 8. Measured average $\delta^{18}O(Zrn)$ values and equilibrium $\delta^{18}O(WR)$ values calculated for host magmas vs SiO_2 content of the whole-rock sample. The $\delta^{18}O(WR)$ of the host magma in equilibrium with zircon was calculated using $\Delta^{18}O(Zrn-WR)$ based on (1) Lackey *et al.* (2008) [equation (1), white triangles] and (2) Bucholz *et al.* (2017) model for dry tholeiitic melt (Bushveld Complex UUMZ, grey triangles), and using the measured SiO_2 wt% (WR) reported in Table 1. The continuous orange and dark blue lines indicate the $\delta^{18}O$ (melt) vs SiO_2 wt% evolutionary trend modeled for the dry Bushveld Complex UUMZ and partly hydrous Dariv igneous complex, respectively (from Bucholz *et al.*, 2017), assuming an initial $\delta^{18}O$ value of 5·6‰ for the parental mantle-derived basaltic melt (Eiler, 2001). The dashed orange and light blue lines indicate the $\delta^{18}O(Zrn)$ values in equilibrium with these evolving melts. The diagonal dark green bar depicts a simplified $\delta^{18}O(melt)$ evolutionary trend for fractional crystallization of uncontaminated MORB magma, used for the calculation of the assimilated altered crust component. The grey horizontal band represents the $\delta^{18}O(Zrn)$ range at high-temperature equilibrium with the mantle (5·3 ± 0·6‰, 2SD; Valley *et al.*, 1998, 2005). The horizontal dashed black line indicates average $\delta^{18}O(Zrn)$ of gabbroic samples from modern slow-spreading mid-ocean ridge environments (Grimes *et al.*, 2011). The tan area at the lower left indicates the SiO_2 and $\delta^{18}O(WR)$ range of hydrothermally altered sheeted-dyke samples from Troodos (Schiffman & Smith, 1988; Vibetti, 1993). For furthere details see Supplementary Data Item S1.

tholeiite series and the use of estimates for liquidus temperatures by Bucholz *et al.* (2017). Thus, equation (1) slightly overestimates $\Delta^{18}O(Zrn-WR)$ whereas the dry UUMZ model underestimates $\Delta^{18}O(Zrn-WR)$. Bucholz *et al.* (2017) also modeled wetter magmas from the Dariv igneous complex of Mongolia and the Kohistan paleo-arc of Pakistan and obtained slightly larger values of $\Delta^{18}O(Zrn-WR)$ at similar SiO_2 content, which are within uncertainty of the model for wet Sierran granitoids by Lackey *et al.* (2008). Determining which $\Delta^{18}O(Zrn-WR)$ model is more suitable for ophiolitic plagiogranites is somewhat ambiguous. Crustal anatexis of hydrothermally altered crust will produce hydrous melts best described by the Lackey *et al.* (2008) model (equation (1)), as done by Grimes *et al.* (2013). However, if these crustal melts are assimilated by voluminous dry tholeiitic magma their combined $\Delta^{18}O(Zrn-$

WR) may be better described by the Bucholz *et al.* (2017) model for the Bushveld UUMZ.

During crystallization of basaltic magma there is a slight increase in $\delta^{18}O(melt)$ as it crystallizes low-$\delta^{18}O$ ferromagnesian silicates, followed by a more rapid increase when Fe–Ti oxides precipitate (Matsuhisa *et al.*, 1973). Thus, advanced fractional crystallization of MORB [initial $\delta^{18}O(WR) = 5\cdot6‰$; Eiler, 2001] should result in an increase of up to ~1–1·5‰ in the $\delta^{18}O(WR)$ values of the evolved felsic magmas (e.g. Muehlenbachs & Byerly, 1982; Wanless *et al.*, 2011). The modelled variation of $\delta^{18}O(WR)$ during closed-system fractional crystallization of Bushveld UUMZ-like and Dariv igneous complex-like magmas evolving from 50 to 75% SiO_2 is shown in Fig. 8 (after Bucholz *et al.*, 2017). These models predict between 1 and 2‰ increase in $\delta^{18}O$ of the plagiogranites relative to the initial MORB value of 5·6‰. The higher than MORB $\delta^{18}O(WR)$ values calculated for most of the Troodos plagiogranites (excluding sample CTE-11B) using hydrous magmas $\Delta^{18}O(Zrn-WR)$ calculated according to equation (1) are consistent with fractional crystallization of the magmas as their dominant formation process. Nevertheless, these $\delta^{18}O(WR)$ values are slightly (0·2–0·5‰) yet systematically lower than those expected from the fractional crystallization of uncontaminated MORB, assuming 1·5‰ increase of $\delta^{18}O$ for melts evolving from 50 to 75% SiO_2 (Fig. 8). This indicates the involvement of melt with lower $\delta^{18}O$ value, derived from crustal anatexis. If only ~1‰ increase of $\delta^{18}O(WR)$ is assumed for evolving dry tholeiitic melts, as seen in the Bushveld UUMZ (Bucholz *et al.*, 2017), no involvement of low-$\delta^{18}O$ crustal melts is required to account for the $\delta^{18}O(WR)$ calculated for most plagiogranite samples using equation (1). However, if zircon is crystallizing from such dry melts, their $\Delta^{18}O(Zrn-WR)$ is expected to be smaller owing to higher temperatures of zircon growth according to the model of Bucholz *et al.* (2017), resulting in lower $\delta^{18}O(WR)$ values for the plagiogranite samples (Fig. 8), which again suggest incorporation of low-$\delta^{18}O$ altered crust or crustal melts.

In the Troodos ophiolite, altered diabase (epidosite) rocks from the base of the sheeted dyke complex yielded $\delta^{18}O(WR)$ values of 2·2–5·4‰ (Vibetti, 1993). Based on $\delta^{18}O(WR)$ values calculated using equation (1), and assuming simple mixing between a hydrothermally altered crustal component with minimal $\delta^{18}O(WR)$ value of 2‰ and an uncontaminated fractionated MORB component with an O isotopic evolution trend of 0·06‰/%SiO_2 [as done by Grimes *et al.* (2013) for plagiogranites of the Oman ophiolite and other ophiolites worldwide], 0–24% (average 9%) assimilation of altered crust is required to produce the range of $\delta^{18}O(WR)$ values calculated for the Troodos plagiogranite magmas (Supplementary Data Item S1). These values are consistent with those estimated for ophiolitic plagiogranites (0–20%) by Grimes *et al.* (2013). It is also consistent with the inferred volume of assimilated hydrothermally altered crust required to explain

chlorine concentrations and O isotope ratios in high-SiO$_2$ andesitic and dacitic lavas of the East Pacific Rise (Wanless *et al.*, 2011). Calculating δ^{18}O(WR) values according to the dry tholeiitic model of Bucholz *et al.* (2017) and assuming simple mixing between a hydrothermally altered crustal component with minimal δ^{18}O(WR) value of 2‰ and an uncontaminated fractionated MORB component with an O isotopic evolution trend of 0·04‰/%SiO$_2$ (as modeled for the Bushveld UUMZ), 9–33% (average 20%) assimilation of altered crust is required to produce the range of δ^{18}O(WR) values calculated for the Troodos plagiogranite magmas (Supplementary Data Item S1). The highest percentage of crustal assimilation, between 24 and 33%, is calculated for sample CTE-11B from the Kakopetria intrusion. If much higher δ^{18}O(WR) values of ∼5‰, similar to the highest values reported by Vibetti (1993), are assumed for the altered crust component, or if it is assumed to be highly fractionated, its amount may be calculated to reach 100%.

In Figure 9 the whole-rock Zr and Sm contents of the Troodos plagiogranites measured by Freund *et al.* (2014) are compared with those measured in leucosomes within a contact aureole at the base of the sheeted dykes complex by Gillis & Coogan (2002). This is done on a plot of Zr—an incompatible element that generally increases with magma evolution—versus Zr/Sm—a ratio of two elements that have disparate incompatibility depending on the magmatic process. Freund *et al.* (2014) noted that most of their plagiogranite samples have near-constant Zr/Sm ratios, lower than those modeled by them for partial melting of a hydrothermally altered sheeted dyke rock containing 40% amphibole. Leucocratic veins and patches of Gillis & Coogan (2002), which are interpreted as partial melts extracted from the hydrothermally altered crust, reach higher Zr/Sm ratios and show a general Zr/Sm enrichment trend consistent with that modeled by Freund *et al.* (2014) for partial melting of hydrothermally altered rocks. The relatively low and constant Zr/Sm ratios observed in their samples (in addition with major element variations) led Freund *et al.* (2014) to conclude that fractional crystallization of mafic melts is the dominant process in forming the Troodos plagiogranites. However, a gentle increasing trend of Zr/Sm ratios with Zr content seen within both their Spilia group and Zoopigi group samples follows the trend seen in the leucocratic veins and patches of Gillis & Coogan (2002), indicating the importance of altered-crust partial melting.

Implications for the Troodos ophiolite tectonic setting

As in many other ophiolites, average δ^{18}O(Zrn) values in Troodos plagiogranites are lower than those found in plagiogranite bodies from modern MOR settings, possibly indicating higher degrees of hydrothermally altered crust remelting (Grimes *et al.*, 2013). Aldiss (1981) also noted that the total volume of plagiogranite
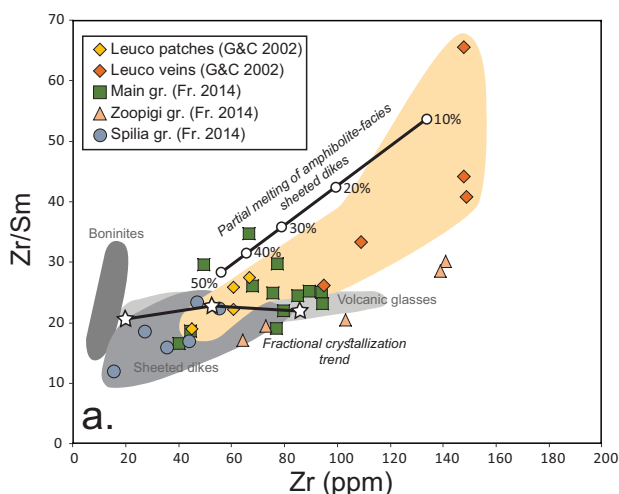
Fig. 9. Zr/Sm ratio vs Zr (ppm) for whole-rock plagiogranite samples (Freund *et al.*, 2014) and leucocratic veins and patches within the contact aureole at the base of the sheeted dykes complex (Gillis & Coogan, 2002; G&C 2002). Also shown are the modeled fractional crystallization evolution trend of mafic magma (open stars) and the evolution trend of melts derived by partial melting of amphibolite-facies metamorphosed sheeted dikes (open circles) (Freund *et al.*, 2014; Fr 2014). The tan colored area marks the extent of all leucocratic samples. The grey shaded areas show the extent of mafic boninites, sheeted dykes and volcanic glass samples (Freund *et al.*, 2014, and references therein).

sampled by dredge and drilling of modern seafloor is small compared with those observed in ophiolites, and Grimes *et al.* (2013) further noted that large-scale plagiogranite bodies, like those found at the Semail ophiolite of Oman, have not been identified at modern ridges.

Grimes *et al.* (2013) suggested that the general difference in δ^{18}O(Zrn) between modern MOR plagiogranites and ophiolitic plagiogranites may be explained by biased sampling of modern plagiogranites from the gabbroic portions of slow-spreading ocean crust exhumed below lithospheric-scale detachment faults in oceanic core complexes. According Grimes *et al.* (2013), in these environments migration of hydrothermal fluids to the depth of magma intrusion is exceedingly restricted (e.g. Alt & Bach, 2006; McCaig & Harris, 2012), leading to limited remelting of hydrothermally altered crust. In contrast, in magmatically active, fast-spreading MOR environments, such as those inferred for the Oman ophiolite (e.g. France *et al.*, 2009) the hydrothermal and magmatic systems occur in closer proximity with temporal overlaps, leading to higher amounts of hydrothermally altered crust melting (Grimes *et al.*, 2013). Consequently, the variation in δ^{18}O(Zrn) seen in plagiogranites from ophiolites (and modern MOR environments) may be related to local spreading rates and magma supply. Lower δ^{18}O(Zrn) values indicate a higher proportion of altered crust remelting in fast-spreading environments, whereas higher δ^{18}O(Zrn) MORB-equilibrium values indicate negligible amount of altered crust assimilation in slow-spreading environments (Grimes *et al.*, 2013).

According to this inferred relation, the relatively low $\delta^{18}O(Zrn)$ values measured here for the Troodos plagiogranites indicate a magmatically active oceanic environment, similar to that envisioned for the Oman ophiolite and fast-spreading MOR segments along the East Pacific Rise (France *et al.*, 2009, 2010; Wanless *et al.*, 2010, 2011).

The spreading rate of the Troodos ophiolite has been a matter of debate. Some studies have suggested a slow-spreading environment with substantial phases of amagmatic spreading and possible formation of an oceanic core complex along the spreading axis (e.g. Varga & Moores, 1985; Hurst *et al.*, 1994; Abelson *et al.*, 2001; Nuriel *et al.*, 2009), whereas others have suggested an intermediate- to fast-spreading environment with magmatic accretion generally keeping pace with tectonic spreading except for brief episodes of amagmatic extension that developed mostly off-axis (e.g. Varga & Moores, 1990; Allerton & Vine, 1991; Van Everdingen & Cawood, 1995). Gillis & Coogan (2002) argued for a high degree (up to ~30 %) of partial melting at the base of the sheeted dyke complex in Troodos and concluded that it indicates the existence of a relatively shallow axial magma chamber, similar to that of a fast-spreading ridge axis. Our data, indicating a substantial component of crustal melt in the Troodos plagiogranitic magmas, seem to support this conclusion. The apparent contradiction between the existence of a shallow axial magma chamber typical of a fast-spreading ridge, inferred by the high percentage of crustal melting (e.g. Gillis & Coogan, 2002), and the evidence for slow spreading along the Troodos ridge axis (e.g. Varga & Moores, 1985; Hurst *et al.*, 1994) may be reconciled by episodes of relatively intense magmatism within an otherwise slow-spreading, magmatically deprived ridge axis. Such episodes of intense magmatic activity could have led to upward migration of the magma chamber, or formation of a new magma chamber where none existed before, which brought about substantial remelting of altered crust. This mechanism may explain the occurrence of relatively low $\delta^{18}O(Zrn)$ values in plagiogranites from a slow-spreading MOR environment, as seen in Troodos.

CONCLUSIONS

1. Oceanic magmatism in the Troodos ophiolite took place at $94 \cdot 3 \pm 0 \cdot 5$ Ma, about 3 Myr earlier than previously recognized. Most of the Troodos plagiogranitic rocks were subjected to later hydrothermal alteration, which resulted in new growth and/or partial alteration of zircon domains, leading to apparently younger bulk-zircon crystallization ages.
2. The new age inferred here for oceanic crust formation in Troodos is closer to that of the Semail ophiolite in Oman, strengthening previous indications for a common tectonic setting for the two ophiolites.

3. Values of $\delta^{18}O(Zrn)$ in the Troodos plagiogranites range between $4 \cdot 2$ and $4 \cdot 8 \permil$, systematically lower than those expected in equilibrium with MORB ($5 \cdot 3 \pm 0 \cdot 6 \permil$). These values are best explained by remelting and assimilation of crust altered by hydrothermal fluids with seawater-like isotopic compositions at high temperatures. Variable amounts of low-$\delta^{18}O$ (~2 ‰) hydrothermally altered crustal component, up to 24–33 %, are required to account for the range of $\delta^{18}O(Zrn)$ in the Troodos plagiogranites. Assuming a higher $\delta^{18}O$ value for the altered crust will require a larger amount of this component.
4. The substantial degree of crustal remelting indicated by the Troodos plagiogranites $\delta^{18}O(Zrn)$ values supports a magmatically active oceanic spreading environment characterized by a relatively shallow magma chamber in close proximity to the hydrothermal system.
5. The existence of a shallow axial magma chamber, typical of fast-spreading MOR settings, within the Troodos slow-spreading ridge axis may indicate episodes of relatively intense magmatic activity.

SUPPLEMENTARY DATA

Supplementary data are available at *Journal of Petrology* online.

REFERENCES

Abelson, M., Baer, G. & Agnon, A. (2001). Evidence from gabbro of the Troodos ophiolite for lateral magma transport along a slow-spreading mid-ocean ridge. *Nature* **409**, 72–75.

Aldiss, D. (1981). Plagiogranites from the ocean crust and ophiolites. *Nature* **289**, 577–578.

Allerton, S. & Vine, F. J. (1991). Spreading evolution of the Troodos ophiolite. *Geology* **19**, 637–640.

Alt, J. C. & Bach, W. (2006). Oxygen isotope composition of a section of lower oceanic crust, ODP Hole 735B. *Geochemistry, Geophysics, Geosystems* **7**, Q12008.

Anenburg, M., Katzir, Y., Rhede, D., Jöns, N. & Bach, W. (2015). Rare earth element evolution and migration in plagiogranites: a record preserved in epidote and allanite of the Troodos ophiolite. *Contributions to Mineralogy and Petrology* **169**, 25.

Baksi, A. K. (2006). A quantitative tool for detecting alteration in undisturbed rocks and minerals—I: water, chemical weathering and atmospheric argon. In: Foulger, G. R. and Jurdy, D. M. (eds) *The Origin of Melting Anomalies, Plates, Plumes and Planetary Processes*. Geological Society of America, Special Publications **430**, 285– 303.

Beccaluva, L., Chinchilla-Chaves, A. L., Coltorti, M., Giunta, G., Siena, F. & Vaccaro, C. (1999). Petrological and structural significance of the Santa Elena-Nicoya ophiolitic complex in Costa Rica and geodynamic implications. *European Journal of Mineralogy* **11**, 1091–1107.

Black, L. P., Kamo, S. L., Allen, C. M., Davis, D. W., Aleinikoff, J. N., Valley, J. W., Mundil, R., Campbell, I. H., Korsch, R. J., Williams, I. S. & Foudoulis, C. (2004). Improved $^{206}Pb/^{238}U$ microprobe geochronology by the monitoring of a trace-element-related matrix effect; SHRIMP, ID-TIMS, ELA-ICP-MS and oxygen isotope documentation for a series of zircon standards. *Chemical Geology* **205**, 115–140.

Bowman, J. R., Moser, D. E., Valley, J. W., Wooden, J. L., Kita, N. T. & Mazdab, F. K. (2011). Zircon U–Pb isotope, $\delta^{18}O$ and trace element response to 80 my of high temperature metamorphism in the lower crust: sluggish diffusion and new records of Archean craton formation. *American Journal of Science* **311**, 719–772.

Brophy, J. G. (2009). La–SiO_2 and Yb–SiO_2 systematics in mid-ocean ridge magmas: implications for the origin of oceanic plagiogranite. *Contributions to Mineralogy and Petrology* **158**, 99–111.

Brophy, J. G. & Pu, X. (2012). Rare earth element–SiO_2 systematics of mid-ocean ridge plagiogranites and host gabbros from the Fournier oceanic fragment, New Brunswick, Canada. *Contributions to Mineralogy and Petrology* **164**, 191–204.

Bucholz, C. E., Jagoutz, O., VanTongeren, J. A., Setera, J. & Wang, Z. (2017). Oxygen isotope trajectories of crystallizing melts: insights from modeling and the plutonic record. *Geochimica et Cosmochimica Acta* **207**, 154–184.

Cameron, W. E. (1985). Petrology and origin of primitive lavas from the Troodos ophiolite. *Contributions to Mineralogy and Petrology* **89**, 239–255.

Cameron, W. E., Nisbet, E. G. & Dietrich, V. J. (1979). Boninites, komatiites and ophiolitic basalts. *Nature* **280**, 550–555.

Cavosie, A. J., Kita, N. T. & Valley, J. W. (2009). Primitive oxygen isotope ratio recorded in magmatic zircons from the Mid-Atlantic Ridge. *American Mineralogist* **94**, 926–934.

Cherniak, D. J. & Watson, E. B. (2001). Pb diffusion in zircon. *Chemical Geology* **172**, 5–24.

Cherniak, D. J. & Watson, E. B. (2003). Diffusion in zircon. In: Hanchar, J. M., and Hoskin, P. W. O. (eds) *Zircon. Mineralogical Society of America and Geochemical Society, Reviews in Mineralogy and Geochemistry* **53**, 113–143.

Coble, M. A., Vazquez, J. A., Barth, A. P., Wooden, J., Burns, D., Kylander-Clark, A., Jackson, S. & Vennari, C. E. (2018). Trace element characterisation of MAD-559 zircon reference material for ion microprobe analysis. *Geostandards and Geoanalytical Research* **42**, 481–497.

Coleman, R. & Donato, M. (1979). Oceanic plagiogranite revisited. In: Barker, F. (ed), *Developments in Petrology,* Volume 6, Trondhjemites, Dacites and related rocks. Elsevier, Amsterdam pp. 149–168.

Coleman, R. G. & Peterman, Z. E. (1975). Oceanic plagiogranite. *Journal of Geophysical Research* **80**, 1099–1108.

Constantinou, G. (1995). *Geological Map of Cyprus, Scale 1: 250,000*. Lefkosia: Geological Survey Department, Cyprus.

Dilek, Y. & Flower, M. F. (2003). Arc–trench rollback and forearc accretion: 2. A model template for ophiolites in Albania, Cyprus, and Oman. In: Dilek, Y. & Robinson, P. T. (eds), *Geological Society, London, Special Publications* **218**, Ophiolites in Earth History, 43–68.

Dilek, Y. & Furnes, H. (2009). Structure and geochemistry of Tethyan ophiolites and their petrogenesis in subduction roll-back systems. *Lithos* **113**, 1–20.

Dilek, Y. & Furnes, H. (2014). Ophiolites and their origins. *Elements* **10**, 93–100.

Eiler, J. M. (2001). Oxygen isotope variations of basaltic lavas and upper mantle rocks. In: Valley, J. W. and Cole, D. R. (eds) *Mineralogical Society of America and Geochemical Society, Reviews in Mineralogy and Geochemistry* **43**, Stable Isotope Geochemistry, 319–364.

Flagler, P. A. & Spray, J. G. (1991). Generation of plagiogranite by amphibolite anatexis in oceanic shear zones. *Geology* **19**, 70–73.

France, L., Ildefonse, B. & Koepke, J. (2009). Interactions between magma and hydrothermal system in Oman ophiolite and in IODP Hole 1256D: fossilization of a dynamic melt lens at fast spreading ridges. *Geochemistry, Geophysics, Geosystems* **10**, Q10O19.

France, L., Koepke, J., Ildefonse, B., Cichy, S. B. & Deschamps, F. (2010). Hydrous partial melting in the sheeted dike complex at fast spreading ridges: experimental and natural observations. *Contributions to Mineralogy and Petrology* **160**, 683–704.

Freund, S., Haase, K. M., Keith, M., Beier, C. & Garbe-Schönberg, D. (2014). Constraints on the formation of geochemically variable plagiogranite intrusions in the Troodos Ophiolite, Cyprus. *Contributions to Mineralogy and Petrology* **167**, 1–22.

Gass, I. G. (1968). Is the Troodos Massif of Cyprus a fragment of Mesozoic Ocean floor? *Nature* **220**, 39–42.

Gillis, K. M. (2002). The rootzone of an ancient hydrothermal system exposed in the Troodos ophiolite. *Journal of Geology* **110**, 57–74.

Gillis, K. M. & Coogan, L. A. (2002). Anatectic migmatites from the roof zone of an ocean ridge magma chamber. *Journal of Petrology* **43**, 2075–2095.

Gregory, R. T. & Taylor, H. P. (1981). An oxygen isotope profile in a section of Cretaceous oceanic crust, Samail Ophiolite, Oman: evidence for $\delta^{18}O$ buffering of the oceans by deep (>5 km) seawater-hydrothermal circulation at mid-ocean ridges. *Journal of Geophysical Research: Solid Earth* **86**, B4.

Grimes, C. B., John, B. E., Kelemen, P. B., Mazdab, F. K., Wooden, J. L., Cheadle, M. J., Hanghøj, K. & Schwartz, J. J. (2007). Trace element chemistry of zircons from oceanic crust: a method for distinguishing detrital zircon provenance. *Geology* **35**, 643–646.

Grimes, C. B., John, B. E., Cheadle, M. J. & Wooden, J. L. (2008). Protracted construction of gabbroic crust at a slow spreading ridge: constraints from $^{206}Pb/^{238}U$ zircon ages from Atlantis Massif and IODP Hole U1309D (30°N, MAR). *Geochemistry, Geophysics, Geosystems* **9**, Q08012.

Grimes, C. B., John, B. E., Cheadle, M. J., Mazdab, F. K., Wooden, J. L., Swapp, S. & Schwartz, J. J. (2009). On the occurrence, trace element geochemistry, and crystallization history of zircon from *in situ* ocean lithosphere. *Contributions to Mineralogy and Petrology* **158**, 757–783.

Grimes, C. B., Ushikubo, T., John, B. E. & Valley, J. W. (2011). Uniformly mantle-like $\delta^{18}O$ in zircons from oceanic

plagiogranites and gabbros. *Contributions to Mineralogy and Petrology* **161**, 13–33.

Grimes, C. B., Ushikubo, T., Kozdon, R. & Valley, J. W. (2013). Perspectives on the origin of plagiogranite in ophiolites from oxygen isotopes in zircon. *Lithos* **179**, 48–66.

Hoskin, P. W. O. (2005). Trace-element composition of hydrothermal zircon and the alteration of Hadean zircon from the Jack Hills. *Geochimica et Cosmochimica Acta* **69**, 637–648.

Hurst, S. D., Moores, E. M. & Varga, R. J. (1994). Structural and geophysical expression of the Solea graben, Troodos ophiolite. *Tectonics* **13**, 139–156.

Ireland, T. R. & Williams, I. S. (2003). Considerations in zircon geochronology by SIMS. In: Hanchar, J. M. and Hoskin, P. W. O. (eds) *Zircon. Mineralogical Society of America and Geochemical Society, Reviews in Mineralogy and Geochemistry* **53**, 215–241.

Kelley, D. S., Robinson, P. T. & Malpas, J. G. (1992). Processes of brine generation and circulation in the oceanic crust: fluid inclusion evidence from the Troodos ophiolite. *Journal of Geophysical Research* **97**, 9307–9322.

Kinnaird, T. C., Robertson, A. H. F. & Morris, A. (2011). Timing of uplift of the Troodos Massif (Cyprus) constrained by sedimentary and magnetic polarity evidence. *Journal of the Geological Society, London* **168**, 457–470.

Kita, N. T., Ushikubo, T., Fu, B. & Valley, J. W. (2009). High precision SIMS oxygen isotope analysis and the effect of sample topography. *Chemical Geology* **264**, 43–57.

Klein, E. M. & Langmuir, C. H. (1987). Global correlations of ocean ridge basalt chemistry with axial depth and crustal thickness. *Journal of Geophysical Research* **92**, 8089–8115.

Koepke, J., Berndt, J., Feig, S. T. & Holtz, F. (2007). The formation of SiO_2-rich melts within the deep oceanic crust by hydrous partial melting of gabbros. *Contributions to Mineralogy and Petrology* **153**, 67–84.

Lackey, J. S., Valley, J. W., Chen, J. H. & Stockli, D. F. (2008). Dynamic magma systems, crustal recycling, and alteration in the central Sierra Nevada batholith: the oxygen isotope record. *Journal of Petrology* **49**, 1397–1426.

Lippard, S. J., Shelton, A. W. & Gass, I. G. (1986). *The Ophiolite of Northern Oman*. Oxford: Blackwell Scientific.

Ludwig, K. (2012). User's Manual for ISOPLOT version 3.75-4.15. A geochronological toolkit for Microsoft Excel. *Berkeley Geochronology Center Special Publication*, **5**, 71 pp.

MacLeod, C., Allerton, S., Gass, I. & Xenophontos, C. (1990). Structure of a fossil ridge–transform intersection in the Troodos ophiolite. *Nature* **348**, 717–720.

Malpas, J. (1979). Two contrasting trondhjemite associations from transported ophiolites in Western Newfoundland: initial report. In: Barker, F. (ed), *Developments in Petrology, Volume 6, Trondhjemites, Dacites and related rocks.* Elsevier, Amsterdam, pp, 465–487.

Malpas, J., Brace, T. & Dunsworth, S. (1989). Structural and petrological relationships of the CY-4 drill hole of the Cyprus Crustal Study Project. In: Gibson, I. L., Malpas, J., Robinson, P. T. & Xenophontos, C. (eds), *Cyprus Crustal Study Project, Hole CY-4: Geological Survey of Canada Paper*, 88–89, 39–67.

Matsuhisa, Y., Matsubaya, O. & Sakai, H. (1973). Oxygen isotope variations in magmatic differentiation processes of the volcanic rocks in Japan. *Contributions to Mineralogy and Petrology* **39**, 277–288.

McCaig, A. M. & Harris, M. (2012). Hydrothermal circulation and the dike–gabbro transition in the detachment mode of slow seafloor spreading. *Geology* **40**, 367–370.

McCallum, J. E. & Robertson, A. H. F. (1990). Pulsed uplift of the Troodos Massif—Evidence from the Plio-Pleistocene Mesaoria Basin. In: Moores, E. M., Malpas, J., Panayiotou, A. and Xenophontos, C. (eds) *Ophiolites: Crustal Analogues. Proceedings of the International Symposium 'Troodos 1987'*. Nicosia: Cyprus Geological Survey Department, pp. 217–230.

McDonough, W. F. & Sun, S. S. (1995). The composition of the Earth. *Chemical Geology* **120**, 223–253.

Moores, E. M. & Vine, F. J. (1971). The Troodos Massif, Cyprus and other Ophiolites as Oceanic Crust: Evaluation and Implications. *Philosophical Transactions of the Royal Society of London* **268**, 443–466.

Morag, N., Haviv, I. & Katzir, Y. (2016). From ocean depths to mountain tops: uplift of the Troodos ophiolite (Cyprus) constrained by low-temperature thermochronology and geomorphic analysis. *Tectonics* **35**, 622–637.

Muehlenbachs, K. & Byerly, G. (1982). δ^{18}O-enrichment of silicic magmas caused by crystal fractionation at the Galapagos spreading center. *Contributions to Mineralogy and Petrology* **79**, 76–79.

Muehlenbachs, K. & Clayton, R. N. (1976). Oxygen isotope composition of the oceanic crust and its bearing on seawater. *Journal of Geophysical Research* **81**, 4365–4369.

Mukasa, S. B. & Ludden, J. N. (1987). Uranium–lead isotopic ages of plagiogranites from the Troodos ophiolite, Cyprus, and their tectonic significance. *Geology* **15**, 825–828.

Nuriel, P., Katzir, Y., Abelson, M., Valley, J. W., Matthews, A., Spicuzza, M. J. & Ayalon, A. (2009). Fault-related oceanic serpentinization in the Troodos ophiolite, Cyprus: implications for a fossil oceanic core complex. *Earth and Planetary Science Letters* **282**, 34–46.

Osozawa, S., Shinjo, R., Lo, C. H., Jahn, B. M., Hoang, N., Sasaki, M., Ishikawa, K., Kano, H., Hoshi, H., Xenophontos, C. & Wakabayashi, J. (2012). Geochemistry and geochronology of the Troodos ophiolite: an SSZ ophiolite generated by subduction initiation and an extended episode of ridge subduction? *Lithosphere* **4**, 497–510.

Pearce, J. A. & Robinson, P. T. (2010). The Troodos ophiolitic complex probably formed in a subduction initiation, slab edge setting. *Gondwana Research* **18**, 60–81.

Pearce, J. A., Lippard, S. J. & Roberts, S. (1984). Characteristics and tectonic significance of supra-subduction zone ophiolites. In: Kokelaar, B. P. &, Howells, M. F. (eds) *Geological Society, London, Special Publications* **16**, Marginal Basin Geology: Volcanic and Associated Sedimentary and Tectonic Processes in Modern and Ancient Marginal Basins, 77–94.

Pedersen, R. B. & Malpas, J. (1984). The origin of oceanic plagiogranites from the Karmoy ophiolite, western Norway. *Contributions to Mineralogy and Petrology* **88**, 36–52.

Rioux, M., Garber, J., Bauer, A., Bowring, S., Searle, M., Kelemen, P. & Hacker, B. (2016). Synchronous formation of the metamorphic sole and igneous crust of the Semail ophiolite: New constraints on the tectonic evolution during ophiolite formation from high-precision U–Pb zircon geochronology. *Earth and Planetary Science Letters* **451**, 185–195.

Robertson, A. H. F. (1977). Tertiary uplift history of the Troodos massif, Cyprus. *Geological Society of America Bulletin* **88**, 1763–1772.

Robertson, A. H. F. (2002). Overview of the genesis and emplacement of Mesozoic ophiolites in the Eastern Mediterranean Tethyan region. *Lithos* **65**, 1–67.

Robinson, P. T., Melson, W. G., O'Hearn, T. & Schmincke, H. U. (1983). Volcanic glass compositions of the Troodos ophiolite. *Geology* **11**, 400–404.

Schiffman, P. & Smith, B. M. (1988). Petrology and oxygen isotope geochemistry of a fossil seawater hydrothermal

system within the Solea graben, northern Troodos ophiolite. *Journal of Geophysical Research: Solid Earth* **93**, 4612–4624.

Schwartz, J. J., John, B. E., Cheadle, M. J., Miranda, E. A., Grimes, C. B., Wooden, J. L. & Dick, H. J. B. (2005). Dating the growth of oceanic crust at a slow-spreading ridge. *Science* **310**, 654–657.

Schwartz, J. J., John, B. E., Cheadle, M. J., Wooden, J. L., Mazdab, F., Swapp, S. & Grimes, C. B. (2010). Dissolution–reprecipitation of igneous zircon in mid-ocean ridge gabbro, Atlantis Bank, Southwest Indian Ridge. *Chemical Geology* **274**, 68–81.

Stacey, J. T. & Kramers, J. (1975). Approximation of terrestrial lead isotope evolution by a two-stage model. *Earth and Planetary Science Letters* **26**, 207–221.

Staudigel, H., Tauxe, L., Gee, J. S., Bogaard, P., Haspels, J., Kale, G., Leenders, A., Meijer, P., Swaak, B., Tuin, M., Van Soest, M. C., Verdurmen, E. A. T. & Zevenhuizen, A. (2000). Geochemistry and intrusive directions in sheeted dikes in the Troodos ophiolite: implications for mid-ocean ridge spreading centers. *Geochemistry, Geophysics, Geosystems* **1**, 1.

Tilton, G. R., Hopson, C. A. & Wright, J. E. (1981). Uranium–lead isotopic ages of the Samail Ophiolite, Oman, with applications to Tethyan ocean ridge tectonics. *Journal of Geophysical Research: Solid Earth* **86**, 2763–2775.

Valley, J. W. (2003). Oxygen isotopes in zircon. In: Hanchar, J. M. and Hoskin, P. W. O. (eds) *Zircon. Mineralogical Society of America and Geochemical Society, Reviews in Mineralogy and Geochemistry* **53**, 343–385.

Valley, J. W., Kinny, P. D., Schulze, D. J. & Spicuzza, M. J. (1998). Zircon megacrysts from kimberlite: oxygen isotope variability among mantle melts. *Contributions to Mineralogy and Petrology* **133**, 1–11.

Valley, J. W., Bindeman, I. N. & Peck, W. H. (2003). Empirical calibration of oxygen isotope fractionation in zircon. *Geochimica et Cosmochimica Acta* **67**, 3257–3266.

Valley, J. W., Lackey, J. S., Cavosie, A. J., Clechenko, C. C., Spicuzza, M. J., Basei, M. A. S., Bindeman, I. N., Ferreira, V. P., Sial, A. N., King, E. M., Peck, W. H., Sinha, A. K. & Wei, C. S. (2005). 4·4 billion years of crustal maturation: oxygen isotope ratios of magmatic zircon. *Contributions to Mineralogy and Petrology* **150**, 561–580.

van Everdingen, D. A., Cawood, P. A. (1995). Dyke domains in the Mitsero graben, Troodos ophiolite, Cyprus: an off-axis model for graben formation at a spreading centre. *Journal of the Geological Society, London* **152**, 923–932.

Vantongeren, J. A., Mathez, E. A. & Kelemen, P. B. (2010). A felsic end to Bushveld differentiation. *Journal of Petrology* **51**, 1891–1912.

Varga, R. J. & Moores, E. M. (1985). Spreading structure of the Troodos ophiolite. *Geology* **13**, 846–850.

Varga, R. J. & Moores, E. M. (1990). Intermittent magmatic spreading and tectonic extension in the Troodos ophiolite: implications for exploration for black smoker-type ore deposits. In: Malpas, J., Moores, E. M., Panayiotou, A. and Xenophontos, C. (eds) *Ophiolites: Oceanic Crustal Analogues*. Nicosia: Cyprus Geological Survey Department, pp. 53–64.

Vibetti, N. (1993). Chemical alteration trends, fluid inclusion patterns and stable isotope compositions in the plutonic sequence of the Troodos ophiolite, Cyprus. *Journal of African Earth Sciences (and the Middle East)* **17**, 193–202.

Wang, X. L., Coble, M. A., Valley, J. W., Shu, X. J., Kitajima, K., Spicuzza, M. J. & Sun, T. (2014). Influence of radiation damage on Late Jurassic zircon from southern China: Evidence from *in situ* measurements of oxygen isotopes, laser Raman, U–Pb ages, and trace elements. *Chemical Geology* **389**, 122–136.

Wanless, V. D., Perfit, M. R., Ridley, W. I. & Klein, E. (2010). Dacite petrogenesis on mid-ocean ridges: evidence for oceanic crustal melting and assimilation. *Journal of Petrology* **51**, 2377–2410.

Wanless, V. D., Perfit, M. R., Ridley, W. I., Wallace, P. J., Grimes, C. B. & Klein, E. M. (2011). Volatile abundances and oxygen isotopes in basaltic to dacitic lavas on mid-ocean ridges: the role of assimilation at spreading centers. *Chemical Geology* **287**, 54–65.

Warren, C. J., Parrish, R. R., Waters, D. J. & Searle, M. P. (2005). Dating the geologic history of Oman's Semail ophiolite: Insights from U–Pb geochronology. *Contributions to Mineralogy and Petrology* **150**, 403–422.

Watts, K. E., Coble, M. A., Vazquez, J. A., Henry, C. D., Colgan, J. P. & John, D. A. (2016). Chemical abrasion-SIMS (CA-SIMS) U–Pb dating of zircon from the late Eocene Caetano caldera, Nevada. *Chemical Geology* **439**, 139–151.